Sub-10-fs population inversion in N_2^+ in air lasing through multiple state coupling

Huailiang Xu[1,2,*], Erik Lötstedt[1,*], Atsushi Iwasaki[1] & Kaoru Yamanouchi[1,*]

Laser filamentation generated when intense laser pulses propagate in air has been an attractive phenomenon having a variety of potential applications such as detection and spectroscopy of gases at far distant places. It was discovered recently that the filamentation in air induces 'lasing', showing that electronically excited N_2^+ is population-inverted, exhibiting marked contrast to the common understanding that molecular ions generated by intense laser fields are prepared mostly in their electronic ground states. Here, to clarify the mechanism of the population inversion, we adopt few-cycle laser pulses, and experimentally demonstrate that the lasing at 391 nm occurs instantaneously after N_2^+ is produced. Numerical simulations clarify that the population inversion is realized by the post-ionization couplings among the lowest three electronic states of N_2^+. Our results shed light on the controversy over the mechanism of the air lasing, and show that this post-ionization coupling can be a general mechanism of the atmospheric lasing.

[1] Department of Chemistry, School of Science, The University of Tokyo, 7-3-1 Hongo, Bunkyo-ku, Tokyo 113-0033, Japan. [2] State Key Laboratory on Integrated Optoelectronics, College of Electronic Science and Engineering, Jilin University, Changchun 130012, China. * These authors contributed equally to this work. Correspondence and requests for materials should be addressed to K.Y. (email: kaoru@chem.s.u-tokyo.ac.jp).

Remote generation of population-inverted gain media in air is a promising step towards the realization of bright and coherent atmospheric lasers for various applications such as standoff spectroscopy[1], sensing[2–4] and remote material processing[5]. Several approaches have been developed so far to remotely build up the population inversion of atmospheric constituents, based on which lasing actions in air, popularly referred to as 'air lasing', have been achieved in both backward and forward propagation direction[2–4,6–10]. In the early demonstrations of air lasing actions, both the major atmospheric constituents, that is, molecular oxygen and nitrogen, were employed as the gain media. With the pump of deep-ultraviolet 100 ps pulses at 226 nm, molecular oxygen in air undergoes two-photon dissociation. Subsequent excitation of atomic oxygen fragments via a resonant two-photon process results in the population inversion between the $3p$ and $3s$ levels, giving rise to high-gain amplified spontaneous emission at 845 nm[3]. For neutral nitrogen molecules, both amplified spontaneous emission and seed amplification of the $C^3\Pi_u(v=0) \rightarrow B^3\Pi_g(v=0)$ transition at 337 nm were realized in laser filaments as the result of the population inversion achieved by the excitation schemes of the optically driven electron impact by femtosecond circularly or picosecond linearly polarized pulses[8–10].

Recently, it was reported that coherent narrow-band $B^2\Sigma_u^+$–$X^2\Sigma_g^+$ (v', v'') emissions of nitrogen molecular ions N_2^+ were also observed when pure nitrogen or air was irradiated with intense laser pulses[6,11–13]. These coherent emissions were found to propagate in the forward direction along the pump laser beam and exhibited excellent temporal and spatial coherence properties. It was further revealed that the most probable mechanism behind the coherent emission is the population inversion in the $B^2\Sigma_u^+$ and $X^2\Sigma_g^+$ states of N_2^+, and that nonlinear processes such as four wave mixing and stimulated Raman scattering in the intense laser fields are not involved[14]. Recent studies[6,12] showed that the population inversion occurs on an ultrafast timescale comparable to the pump laser pulse (40–200 fs).

However, the underlying mechanism of building up the population inversion has not been convincingly explained since the first observation of the air lasing with N_2^+ as the gain medium[2,6]. This is because when a nitrogen molecule is exposed to an intense laser field, the ejection of an outer valence electron in the highest occupied molecular orbital (HOMO) of N_2 leaves the ion N_2^+ in the ground $X^2\Sigma_g^+$ state, whereas the ejection of an inner-valence electron in the HOMO-2 leads preferentially to the formation of N_2^+ in the excited $B^2\Sigma_u^+$ state[15]. Since the ionization potential ($I_p = 18.7$ eV)[16] for the removal of the HOMO-2 electron is much larger than that ($I_p = 15.6$ eV)[16] for the removal of the HOMO electron of N_2, it was theoretically predicted that the resultant yield of N_2^+ in the ground $X^2\Sigma_g^+$ state in an intense laser field is much larger than that of N_2^+ in the excited $B^2\Sigma_u^+$ state[17], and thus, the population inversion of N_2^+ would not occur in intense laser fields. Therefore, previous studies mainly focused on the generation of N_2^+ lasing and experimental verification of population inversion[2,6,9–14], and only some conjectures have been proposed for the population inversion mechanism, for example, different electron-ion recombination rates of ions in the $B^2\Sigma_u^+$ state and the $X^2\Sigma_g^+$ state[2], and post-ionization Raman-like excitation[12].

In the present study, we demonstrate the generation of the air lasing of N_2^+ at 391 nm by the irradiation of intense few-cycle 800 nm pulses into air. The formation of self-generated white-light seed amplification in the filamentation of a few-cycle laser pulse implies that it takes only 4–5 fs in achieving the population inversion. We consider various possible mechanisms that may

contribute to the population inversion of N_2^+ and show, based on the results of numerical calculations, that the population inversion can be ascribed to the post-ionization optical coupling in the three-level system formed by the electronic ground state $X^2\Sigma_g^+$ and the electronically excited states $A^2\Pi_u$ and $B^2\Sigma_u^+$ in N_2^+. After ionization of N_2 to produce N_2^+, the field-induced $X^2\Sigma_g^+$–$A^2\Pi_u$ and $X^2\Sigma_g^+$–$B^2\Sigma_u^+$ couplings in the later part of the laser pulse can generate population inversion in the $X^2\Sigma_g^+$ ($v=0$)–$B^2\Sigma_u^+$ ($v=0$) transition. A key factor in the achievement of the population inversion is the presence of the $A^2\Pi_u$ state, which effectively acts as a trap for population transferred from the $X^2\Sigma_g^+$ state through its lower dipole coupling strength.

Results

Experiment. We employ few-cycle laser pulses to produce the 391 nm lasing in ambient air (for experimental details, see Methods). The lasing actions and the excitation scheme of the population inversion of N_2^+ are schematically shown in Fig. 1a. The few-cycle pump pulse has two roles, that is, the ionization of the nitrogen molecules and the establishment of the population inversion of N_2^+. When the few-cycle pulse is focused in air, ionization of nitrogen molecules occurs with the laser intensity clamped inside the filament which is produced as a result of a dynamical interplay between Kerr self-focusing and defocusing of self-generated air plasma[18]. Meanwhile, the refractive index of air in the filament of the intense few-cycle laser pulse is modified, leading to the generation of new frequencies as a result of self-phase modulation[19]. It is found, as shown in Fig. 1b, that when the spectrum of the few-cycle pulse in the blue side becomes broad enough to cover the $B^2\Sigma_u^+(v=0) \rightarrow X^2\Sigma_g^+(v=0)$ transition of N_2^+, the narrow-band emission at 391 nm appears
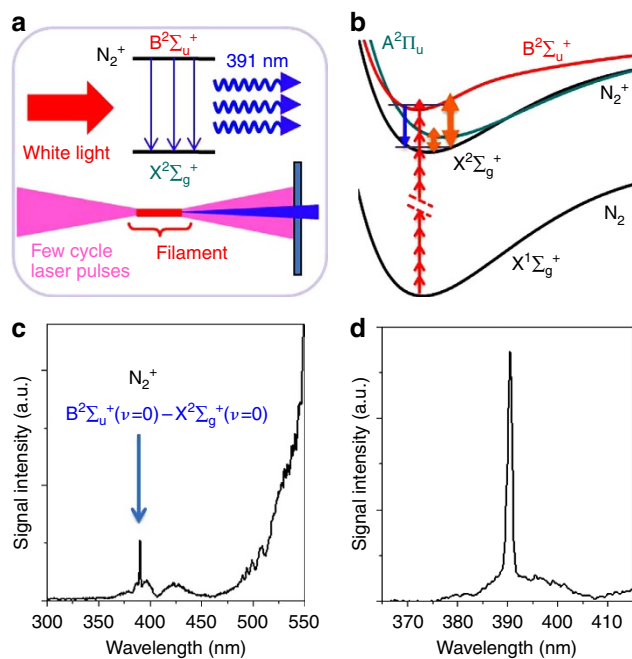

Figure 1 | Air lasing concept and lasing emission. Schematics (**a**) of the lasing actions induced by the few-cycle laser pulse and the excitation scheme (**b**) of the population inversion with the potential energy surfaces[20–22] of N_2^+, in which the upward red arrows denote the 800 nm laser photon, the downward blue arrow the lasing emission at 391 nm, and the double-headed arrows the dipole coupling induced by the laser field. (**c**) Forward spectrum of air lasing recorded together with the white light. (**d**) Spectrum of air lasing recorded forwardly with a band-pass filter.

in the recorded forward laser spectrum. It can be seen from Fig. 1b that the intensity of the 391 nm band is about five times larger than that of the white light laser signal in the spectral range of 350–400 nm and no other fluorescence such as the strongest nitrogen signal at 337 nm can be observed. Our result is similar to the air lasing actions observed with long 40–200 fs pulses as the pump[6,9], showing that the population inversion is achieved by the few-cycle laser pulse. Figure 1c shows the clean lasing spectrum with the white light filtered out by a band-pass filter, which is placed just before the fibre spectrometer.

Theory. In order to simulate the population distribution of N_2^+ ions exposed to an intense laser pulse, we numerically solve the time-dependent Schrödinger equation for the nuclear wave function of N_2^+ (for details of the calculation, see Methods). We assume that at some instant during the laser pulse, an N_2^+ molecular ion is created by the tunnelling ionization of N_2. After the ionization event, the N_2^+ molecular ion is still in the laser pulse, and therefore the field-induced coupling among the electronic states of N_2^+ changes the final populations of the excited states.

Our model includes non-perturbatively the dipole transitions (including resonant and Raman-type transitions) among all vibrational states on the three electronic states $X^2\Sigma_g^+$, $A^2\Pi_u$ and $B^2\Sigma_u^+$. The ground $X^2\Sigma_g^+$ state is coupled to the excited $A^2\Pi_u$ state by the component of the laser field perpendicular to the molecular axis, while the ground state and the $B^2\Sigma_u^+$ state couple via the parallel component. At the equilibrium internuclear distance $r_e \approx 1.12$ Å of the $X^2\Sigma_g^+$ state, the numerical values of the dipole couplings are[20,21] $\langle X^2\Sigma_g^+ | \mu_\perp | A^2\Pi_u \rangle \approx 0.7D$ and $\langle X^2\Sigma_g^+ | \mu_\parallel | B^2\Sigma_u^+ \rangle \approx 1.8D$. Due to the different symmetry, there is no direct coupling between the $B^2\Sigma_u^+$ state and the $A^2\Pi_u$ state. Rotation of the molecule during the interaction with the laser field is neglected, since the rotational period is of N_2 is about 8 ps (ref. 22).

In Fig. 2a, we show an example of the time-dependent populations of the three electronic states, at the laser intensity of 2×10^{14} W cm^{-2}, and where the angle between the laser polarization vector and the molecular axis is $\theta = 45°$. At this value of θ the component of the laser field parallel to the molecular axis equals the perpendicular component, which exemplifies the situation when the $X^2\Sigma_g^+$ state is coupled both to the $A^2\Pi_u$ state and to the $B^2\Sigma_u^+$ state, and leads to a particularly efficient creation of population inversion. We have assumed that tunnelling ionization from N_2 to N_2^+ occurs at $t = 0$ (at the peak of the laser pulse), and that the strong field-induced dynamics starts immediately after the ionization. The initial populations are taken to be proportional to the Ammosov–Delone–Krainov tunnelling rate of ionization[17,23] to the respective electronic state. For the nuclear wave function, we adopted the Franck–Condon approximation and assumed the initial nuclear wave function to be identical to that of the vibrational ground state of N_2. To make comparison with experiment, we average the final populations over the ionization time and over the alignment angle θ (assuming a randomly aligned molecular ensemble). The result of such an averaging is shown in Fig. 2b. In this figure, we also show a curve where we include only direct tunnelling ionization without post-ionization coupling.

We have also calculated the post-ionization coupled-state dynamics for a longer laser pulse. In Fig. 3a, we show the result of a calculation employing a pulse with a full-width at half-maximum (FWHM) of 20 fs, at an intensity of 2×10^{14} W cm^{-2} and an alignment angle of $\theta = 45°$. Figure 3b shows the result of averaging over ionization time and alignment angle.
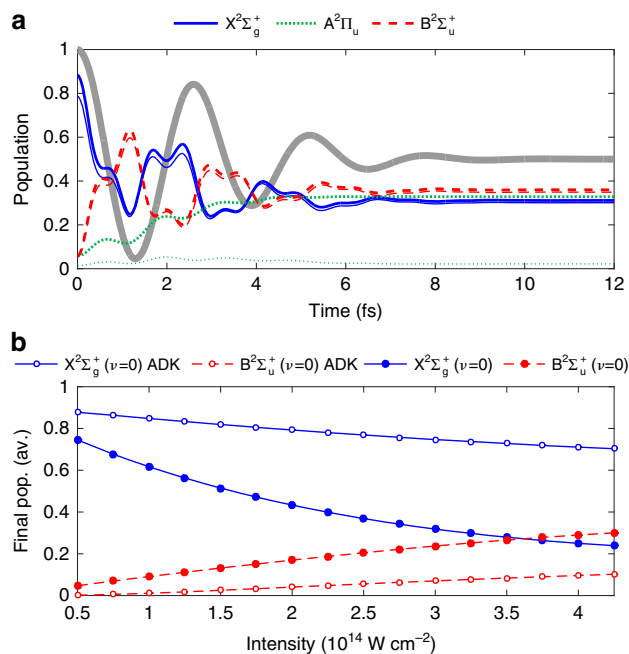

Figure 2 | Population inversion of N_2^+ in a few-cycle laser pulse.
(**a**) Time-dependent populations in the three electronic states, at a field intensity of 2×10^{14} W cm^{-2}, and alignment angle $\theta = 45°$. Thick lines show the total population, while the thin lines show the population in the vibrational ground state. The laser field (not to scale) is indicated in the background as a fat, grey line. (**b**) Final populations averaged over alignment angle and ionization time, in the vibrational ground state of the $X^2\Sigma_g^+$ state (solid lines), and of the $B^2\Sigma_u^+$ state (broken lines). Closed symbols are the result of tunnelling ionization and post-ionization coupling, and open symbols show the result when only tunnelling ionization is included.

Discussion

The laser intensity in the experiments is estimated to be 4.2×10^{14} W cm^{-2}. On the basis of previous measurements by Mitryukovskiy et al.[24], for a collimated or weakly converging laser beam, the clamped intensity is about 1.4×10^{14} W cm^{-2}, and for a tightly focused beam with a 10 cm focal length, the laser intensity is increased by about three times[25]. However, it can be seen in Fig. 2b that direct tunnelling ionization is insufficient to generate population inversion at the laser intensities of 4.2×10^{14} W cm^{-2}.

In the following, we consider several possible scenarios that may contribute to the establishment of the population inversion of N_2^+ in a laser-induced filament. We show that only the mechanism proposed in the current paper, strong field-induced post-ionization coupling of the electronic states, is able to yield population inversion on sub-ps timescale.

The first possibility is that after ionization, N_2^+ molecules in the electronic ground state are excited by colliding with free electrons in the surrounding plasma. This mechanism has been shown to be the dominant one for the population of the $B^2\Sigma_u^+$ state in filaments created by circularly polarized laser pulses[9,10,24]. However, given that the cross-section σ for the reaction $e^- + N_2^+(X^2\Sigma_g^+, v = 0) \rightarrow e^- + N_2^+(B^2\Sigma_u^+, v = 0)$ is of the order of 10^{-16} cm^2 (see ref. 26), and that the typical free electron kinetic energy is $\frac{mv_e^2}{2} \approx 3$eV (ref. 24), the resulting collision rate $R_{coll} = \rho_e v_e \sigma \approx 10^9$ s^{-1} (assuming an electron density $\rho_e = 10^{17}$ cm^{-3} as measured in ref. 25). This means that the collision of the electrons with the surrounding nitrogen ions occurs on a nanosecond timescale, much slower than the duration
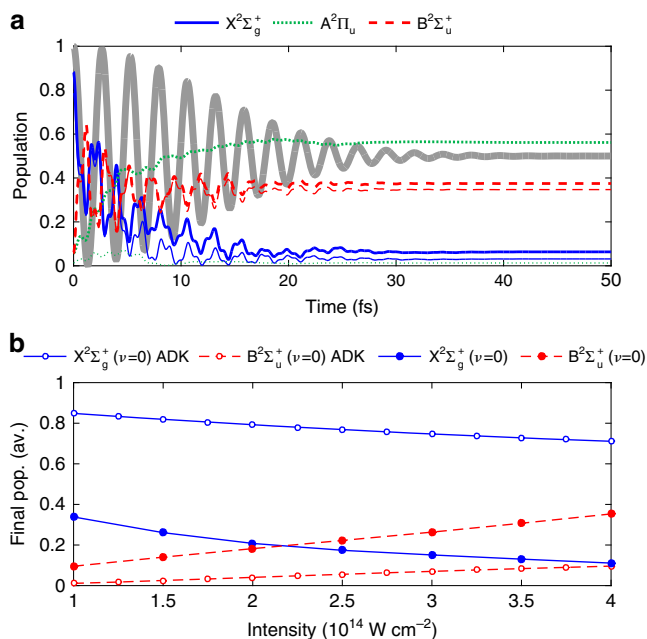
a

b

Figure 3 | Population inversion of N_2^+ in a 20-fs laser pulse. (**a**) Time-dependent populations of the three electronic states in a laser pulse with a FWHM of 20 fs (other laser parameters as in Fig. 2), assuming ionization at $t = 0$. Thick lines represent the total population in all vibrational states, and thin lines correspond to the populations in the vibrational ground states. The laser field (not to scale) is plotted in the background. (**b**) Final populations in the vibrational ground state of the $X^2\Sigma_g^+$ state (solid lines), and of the $B^2\Sigma_u^+$ state (broken lines). We compare the case when only tunnelling ionization is included (open symbols) and when tunnelling ionization and post-ionization dynamics is included (solid symbols).

of a femtosecond laser pulse. Therefore, we can exclude the contribution of this possibility to the ultrafast population inversion observed for the $B^2\Sigma_u^+$ state and the $X^2\Sigma_g^+$ state in N_2^+.

The second possibility which may contribute the population inversion is the recollision[27] of the electron ejected from N_2 with its parent N_2^+ ion, which could excite nitrogen ions from $X^2\Sigma_g^+$ state to $B^2\Sigma_u^+$ ($v = 0$). The size of the recolliding electronic wave packet at recollision can be estimated to be[28] $A \approx \pi^2 e E_0(t_{ion}) \sqrt{\frac{m}{2I_p}} \frac{\hbar}{m^2\omega^2}$. In our case with an ionization potential of $I_p = 15.6\,eV$ and a peak intensity of $4 \times 10^{14}\,W\,cm^{-2}$ we have $A \approx 8 \times 10^{-15}\,cm^2$, much larger than the cross-section $\sigma \approx 10^{-16}\,cm^2$ for the reaction $e^- + N_2^+(X^2\Sigma_g^+, v = 0) \rightarrow e^- + N_2^+(B^2\Sigma_u^+, v = 0)$[26]. By calculating the recollision probability for an ejected electron as $\sigma/A \approx 0.01$, we estimate that the recollision has a negligible contribution to the population inversion of N_2^+.

The third possibility is the 'post-ionization' optical couplings among the electronic excited states. As shown in Fig. 2a, the $X^2\Sigma_g^+$ state and the $B^2\Sigma_u^+$ state are strongly coupled, which results in a large population transfer occurring on a sub-cycle timescale. On the other hand, due to the smaller transition dipole matrix element, the population dynamics in the $A^2\Pi_u$ state is almost unidirectional: population is transferred to the $A^2\Pi_u$ state, but not back to the ground state again. Clearly, the strong field-induced coupling of the electronic states drastically increases the relative population of the $B^2\Sigma_u^+$ state when compared with the results of the direct tunnel ionization, as shown by the open and closed symbols in Fig. 2b. After the laser pulse has passed, population inversion is achieved: the final population in the

$B^2\Sigma_u^+$ ($v = 0$) state is larger than that in the $X^2\Sigma_g^+$ ($v = 0$) state. The calculated population inversion is achieved at a peak field intensity of $3.6 \times 10^{14}\,W\,cm^{-2}$, which is smaller than the laser intensity of $4.2 \times 10^{14}\,W\,cm^{-2}$ estimated from the current experimental condition, and therefore confirms the generation of the population inversion of N_2^+ within a few-cycle pulse. We point out that the average of the final population over the ionization time and over the alignment angle θ leads to an increase of the laser intensity to realize the population inversion as compared with that obtained in Fig. 2a. The reason is that at other alignment angles and ionization times than adopted in Fig. 2a, the population inversion is less efficient.

For the longer pulse case shown in Fig. 3, it can be seen from Fig. 3a that the final population in the $B^2\Sigma_u^+$ ($v = 0$) state is larger than that in the $X^2\Sigma_g^+$ ($v = 0$) state, and the difference of the populations between these two states is much larger when compared with that obtained in Fig. 2a. After the average of the final population over the ionization time and over the alignment angle θ, it can be seen from Fig. 3b that the population inversion can be achieved with a laser intensity of about $2.2 \times 10^{14}\,W\,cm^{-2}$. This lowered intensity for the population inversion indicates the effects of the pulse duration on the population inversion of N_2^+, which may reflect an effectively stronger coupling between the excited state and the ground state of N_2^+ for a longer pulse. As described in ref. 29, the clamping intensity in air becomes higher when the pulse duration decreases from 200 to 42 fs. In the case of 5 or 20 fs pulses, the electronic responses of molecules are much faster, and the laser pulse may propagate with higher intensity, resulting in the higher clamping intensity than in the case of the longer pulse[29]. This is consistent with the threshold intensity of the population inversion shown in Figs 2b and 3b.

To examine the significance of the $A^2\Pi_u$ state, we carried out further simulations for both 5 and 20 fs laser pulses, assuming that there is no coupling between the $X^2\Sigma_g^+$ state and $A^2\Pi_u$ states, that is, the population in the $A^2\Pi_u$ state is kept to be constant after the ionization; meanwhile, keeping all other parameters to be the same as those in the simulations of Figs 2 and 3. For both 5 and 20 fs laser pulses, we find after averaging over alignment angle and ionization time that the population inversion of N_2^+ between the $X^2\Sigma_g^+$ state and $B^2\Sigma_u^+$ state cannot be achieved in the intensity interval of $1 \times 10^{14}\,W\,cm^{-2} \leq I \leq 4 \times 10^{14}\,W\,cm^{-2}$. This result clearly shows the significance of the $A^2\Pi_u$ state, which can be regarded as a trap for the population transferred to the excited $A^2\Pi_u$ state of N_2^+.

We have also considered the contribution from the excited $C^2\Sigma_u^+$ electronic state of N_2^+ in generating the population inversion of N_2^+. The $C^2\Sigma_u^+$ state couples directly to the ground $X^2\Sigma_g^+$ state via a parallel transition, but not to the $A^2\Pi_u$ and $B^2\Sigma_u^+$ states. At the equilibrium internuclear distance of the ground $X^2\Sigma_g^+$ state, the energy gap between the $X^2\Sigma_g^+$ state and the $C^2\Sigma_u^+$ state is[21] $E(C^2\Sigma_u^+) - E(X^2\Sigma_g^+) \approx 9\,eV$, which is larger than $E(B^2\Sigma_u^+) - E(X^2\Sigma_g^+) \approx 3\,eV$ (ref. 21) and $E(A^2\Pi_u) - E(X^2\Sigma_g^+) \approx 1\,eV$ (ref. 20). The dipole matrix element is $\langle X^2\Sigma_g^+ |\mu_\parallel| C^2\Sigma_u^+ \rangle \approx 0.2\,D$. For the same parameters as used in Figs 2 and 3, we solved the Schrödinger equation including the four states $X^2\Sigma_g^+$, $A^2\Pi_u$, $B^2\Sigma_u^+$ and $C^2\Sigma_u^+$, but no significant difference is observed when compared with those shown in Figs 2 and 3. The negligible contribution of the $C^2\Sigma_u^+$ state can be ascribed to the large energetic gap between the $X^2\Sigma_g^+$ and $C^2\Sigma_u^+$ states, leading to a negligible coupling of the ground $X^2\Sigma_g^+$ state with the excited $C^2\Sigma_u^+$ state at the intensity of a few $10^{14}\,W\,cm^{-2}$.

In summary, we have demonstrated that the post-ionization strong field-induced dynamics of the three-level system formed

by the $X^2\Sigma_g^+$, $B^2\Sigma_u^+$ and $A^2\Pi_u$ states in N_2^+ plays a key role in generation of the population inversion of N_2^+. The excited $A^2\Pi_u$ state is essential in the coupling, which serves as a 'population reservoir' in the process of transferring the population into the $B^2\Sigma_u^+$ state and depleting the population from the ground state. The proposed mechanism of post-ionization coupling can explain the formation of population inversion in N_2^+ irradiated with long, ~100 fs laser pulses as employed in previous experiments[6,11–14], but also implies that population inversion can be achieved using ultrashort, few-cycle pulses. We confirm this statement by observing that lasing in air can be produced even for a pulse as short as 4–5 fs.

Methods

Experimental details. We performed experiments with linearly polarized few-cycle laser pulses, which were produced from a femtosecond Ti:sapphire laser system (5 kHz, 0.6 mJ, 800 nm and 30 fs). Output pulses from the Ti:sapphire laser system were focused into a hollow-core fibre (inner diameter: 330 μm, length: 1.5 m) filled with argon gas at the pressure of 470 mbar to broaden the bandwidth of the pulse. After compressing the pulse by a set of chirped mirrors (PC70, Ultrafast Innovations) and two wedges, few-cycle pulses were generated (~6 fs, 5 kHz and 0.2 mJ)[30]. The pulse duration of the few-cycle pulse was measured by an autocorrelator (FEMTOMETER). The generated few-cycle pulse was directly focused by a parabolic mirror ($f = 10$ cm) in air to ionize the air molecules. A single filament of about 3 mm was produced. The forward light after the focus was collected by a lens ($f = 15$ cm) and then focused into a fibre spectrometer (Ocean optics USB 4000-UV-VIS) in a 2f–2f manner.

Numerical calculation. The population dynamics in the N_2^+ molecular ion is calculated by solving the time-dependent Schrödinger equation

$$i\hbar \frac{\partial}{\partial t}\Psi(r,t) = \left(-\frac{\hbar^2}{2\mu}\frac{\partial^2}{\partial r^2} + V_0(r) + E(t)\cos\theta D_{XB}(r) + E(t)\sin\theta D_{XA}(r)\right)\Psi(r,t).$$
(1)

In Equation (1), $\Psi = (\psi_1, \psi_2, \psi_3)^T$ is a column vector containing the nuclear wave functions at the respective electronic surface (we have used the labelling 1 for the $X^2\Sigma_g^+$ state, 2 for the $A^2\Pi_u$ state, and 3 for the $B^2\Sigma_u^+$ state), r is used to denote the internuclear distance, μ is the reduced mass of N_2^+, θ is the angle between the molecular axis and the laser polarization direction, and $E(t) = E_0(t)\cos(\omega t)$ is the laser field. The potential V_0 is a 3×3 diagonal matrix with matrix elements $(V_0)_{ii} = v_i(r)$. The dipole transition matrices D_{XB} and D_{XA} are 3×3 matrices with the only non-vanishing matrix elements being $(D_{XB})_{13} = (D_{XB})_{31} = d_{13}(r)$, and $(D_{XA})_{12} = (D_{XA})_{21} = d_{12}(r)$. The potential energy curves $v_{1,2,3}(r)$ and the transition dipole moments $d_{12,13}(r)$ are taken from refs 20,21. The dipole moment $d_{12}(r)$ changes smoothly from $d_{12}(r = 1\text{ Å}) \approx 0.7$D to $d_{12}(r = 2\text{ Å}) \approx 0.1$D, while $d_{13}(r)$ varies monotonically from $d_{12}(r = 1\text{ Å}) \approx 2.0$D to $d_{12}(r = 2\text{ Å}) \approx -1.0$D.

To solve Equation (1) numerically, the wave functions are discretized on a grid with mesh width $\Delta r = 0.0053$ Å. We use a 3-point finite difference approximation for the kinetic energy operator. The time propagation is accomplished with the split-operator technique, using the Crank–Nicolson algorithm for the time-independent operators, and the Lanczos algorithm for the time-dependent ones, with a time step length of $\delta t = 12$ as.

For all calculations, we employ a Gaussian envelope function $E_0(t)$ with an intensity FWHM of 5 fs, an angular frequency $\omega = 2.4$ rad s^{-1} (corresponding to a wavelength of 800 nm), and a CEP $\phi = 0$. The initial nuclear wave function is taken to be $\Psi(0) = \psi_{N_2}^0(r)[c_1, c_2, c_3]^T$, where $\psi_{N_2}^0(r)$ is the vibrational ground state of the electronic state potential energy curve of the neutral N_2 molecule[22] (The Franck–Condon approximation), and $c_{1,2,3}$ are constants specifying the relative populations of the electronic states.

The total population $P_i(t)$ in state i is defined as $P_i(t) = \int dr |\psi_i(r,t)|^2$, and satisfies $\sum_{i=1}^{3} P_i(t) = 1$ at all times. In a similar way, the population P_i^0 in the vibrational ground state of the electronic state i is calculated as $P_i^0 = \left|\int dr \psi_i^*(r,t)\phi_i^0(r)\right|^2$, where $\phi_i^0(r)$ is the ground state wave function of the potential energy curve i.

An example of the nuclear density $\rho_i(r,t) = |\psi_i(r,t)|^2$ in each electronic state for the same laser parameters as used in Fig. 2a ($I_0 = 2 \times 10^{14}$ W cm^{-2}, $\theta = 45°$, FWHM = 5 fs) is shown in Fig. 4. The strong coupling between the $X^2\Sigma_g^+$ and the $B^2\Sigma_u^+$ states is clearly visible. Also interesting is that since the equilibrium internuclear distance for the $A^2\Pi_u$ state is larger than that of the $X^2\Sigma_g^+$ state (see the potential energy curves in Fig. 1a), vibrational motion is induced following the population transfer to the $A^2\Pi_u$ state. On the other hand, the nuclear wave functions in the $X^2\Sigma_g^+$ state and the $B^2\Sigma_u^+$ state have a large overlap with the respective vibrational ground state.

The averaging over the alignment angle θ and over ionization time t_0 is performed in the following way. We define $\Psi_{ji}^{final}(t_0, \theta)$ as the final nuclear wave function in state i, calculated from an initial wave function given by
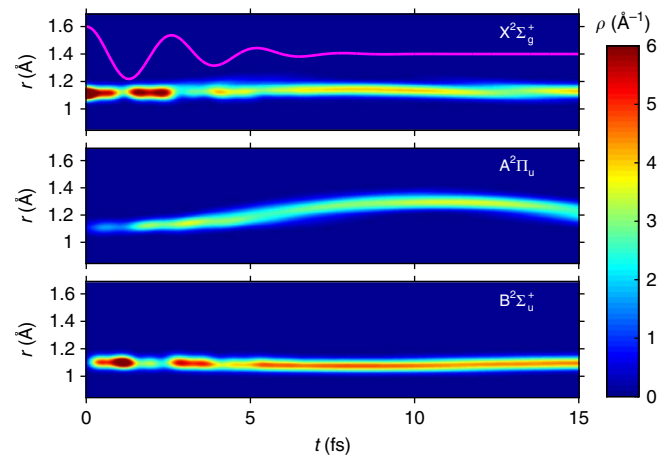

Figure 4 | Time-dependent nuclear density $\rho_i(r, t) = |\psi_i(r, t)|^2$.
Nuclear densities in the $X^2\Sigma_g^+$ state (top), the $A^2\Pi_u$ state (middle) and the $B^2\Sigma_u^+$ state (bottom). The laser parameters used are the same as in Fig. 2a. In the top panel (showing the $X^2\Sigma_g^+$ state), the laser field (on an arbitrary scale) is indicated as a solid line.

$\Psi(0) = \psi_0^{N_2}(r)[c_1, c_2, c_3]^T$, $c_j = 1$, $c_{k\neq j} = 0$ (corresponding to an initial state with population only in state j), and at alignment angle θ. The incoherently averaged population $\bar{P}_i$ is then given by

$$\bar{P}_i = \frac{1}{K}\int_0^\pi \sin\theta\, d\theta \int_{-\infty}^\infty dt \int_0^\infty dr \sum_j W_j^{ADK}(|E(t)|, \theta)\left|\Psi_{ji}^{final}(t, \theta)\right|^2,$$
(2)

where $W_j^{ADK}(F, \theta)$ is the Ammosov–Delone–Krainov ionization rate[17] for tunnelling ionization to N_2^+ in electronic state j, at field strength F and alignment angle θ. K is a normalization constant to assure $\sum_i \bar{P}_i = 1$. In the case of the longer pulse shown in Fig. 3b, the integral over t in Equation (2) is approximated by a sum over the time instants of the laser field peaks. The averaged final populations assuming only tunnelling ionization (shown with open symbols in Fig. 2b) are similarly calculated by integrating $W_j^{ADK}(|E(t)|, \theta)$ over t and θ, and multiplying with the respective Franck–Condon factor.

References

1. Hemmer, P. R. *et al.* Standoff spectroscopy via remote generation of a backward-propagating laser beam. *Proc. Natl Acad. Sci. USA* **108,** 3130–3134 (2011).
2. Luo, Q., Liu, W. & Chin, S. L. Lasing action in air induced by ultra-fast laser filamentation. *Appl. Phys. B* **76,** 337–340 (2003).
3. Dogariu, A., Michael, J. B., Scully, M. O. & Miles, R. B. High-gain backward lasing in air. *Science* **331,** 442–445 (2011).
4. Ni, J. *et al.* Impulsive rotational Raman scattering of N_2 by a remote "air laser" in femtosecond laser filament. *Opt. Lett.* **39,** 2250–2253 (2014).
5. Liu, Y. *et al.* Ciliary white light: optical aspect of ultrashort laser ablation on transparent dielectrics. *Phys. Rev. Lett.* **110,** 097601 (2013).
6. Yao, J. *et al.* High-brightness switchable multiwavelength remote laser in air. *Phys. Rev. A* **84,** 051802(R) (2011).
7. Laurain, A., Scheller, M. & Polynkin, P. Low-threshold bidirectional air lasing. *Phys. Rev. Lett.* **113,** 253901 (2014).
8. Kartashov, D. *et al.* Remotely pumped stimulated emission at 337 nm in atmospheric nitrogen. *Phys. Rev. A* **88,** 041805 (2013).
9. Mitryukovskiy, S., Liu, Y., Ding, P. J., Houard, A. & Mysyrowicz, A. Backward stimulated radiation from filaments in nitrogen gas and air pumped by circularly polarized 800 nm femtosecond laser pulses. *Opt. Express* **22,** 12750–12759 (2014).
10. Yao, J. P. *et al.* Gain dynamics of a free-space nitrogen laser pumped by circularly polarized femtosecond laser pulses. *Opt. Express* **22,** 19005–19013 (2014).
11. Point, G. *et al.* Lasing of ambient air with microjoule pulse energy pumped by a multi-terawatt infrared femtosecond laser. *Opt. Lett.* **39,** 1725–1728 (2014).
12. Yao, J. P. *et al.* Remote creation of coherent emissions in air with two-color ultrafast laser pulses. *New J. Phys.* **15,** 023046 (2013).
13. Zhang, H. S. *et al.* Rotational coherence encoded in an "air-laser" spectrum of nitrogen molecular ions in an intense laser field. *Phys. Rev. X* **3,** 041009 (2013).
14. Ni, J. L. *et al.* Identification of the physical mechanism of generation of coherent N_2^+ emissions in air by femtosecond laser excitation. *Opt. Express* **21,** 8746–8752 (2013).

15. Becker, A., Bandrauk, A. D. & Chin, S. L. S-matrix analysis of non-resonant multiphoton ionisation of inner-valence electrons of the nitrogen molecule. *Chem. Phys. Lett.* **343,** 345–350 (2001).

16. Lofthus, A. & Krupenie, P. H. The spectrum of molecular nitrogen. *J. Phys. Chem. Ref. Data* **6,** 113–307 (1977).

17. Zhao, S. F., Cheng, J., Le, A. T., Jiang, T. F. & Lin, C. D. Determination of structure parameters in strong-field tunneling ionization theory of molecules. *Phys. Rev. A* **81,** 033423 (2010).

18. Chin, S. L. *Femtosecond Laser Filamentation* (Springer, 2010).

19. Bergé, L., Skupin, S., Nuter, R., Kasparian, J. & Wolf, J.-P. Ultrashort filaments of light in weakly ionized, optically transparent media. *Rep. Prog. Phys.* **70,** 1633–1713 (2007).

20. Langhoff, S. R., Bauschlicher, Jr C. W. & Partridge, H. Theoretical study of the N_2^+ Meinel system. *J. Chem. Phys.* **87,** 4716–4721 (1987).

21. Langhoff, S. R. & Bauschlicher, Jr C. W. Theoretical study of the first and second negative systems of N_2^+. *J. Chem. Phys.* **88,** 329–336 (1988).

22. Li, X. & Paldus, J. Full potential energy curve for N_2 by the reduced multireference coupled-cluster method. *J. Chem. Phys.* **129,** 054104 (2008).

23. Ammosov, M. V., Delone, N. B. & Krainov, V. P. Tunnel ionization of complex atoms and of atomic ions in an alternating electromagnetic field. *Sov. Phys. JETP* **64,** 1191–1194 (1986).

24. Mitryukovskiy, S. *et al.* Plasma luminescence from femtosecond filaments in air: evidence for impact excitation with circularly polarized light pulses. *Phys. Rev. Lett.* **114,** 063003 (2015).

25. Theberge, F., Liu, W. W., Simard, Tr. S., Becker, A. & Chin, S. L. Plasma density inside a femtosecond laser filament in air: strong dependence on external focusing. *Phys. Rev. E* **74,** 036406 (2006).

26. Crandall, D. H., Kauppila, W. E., Phaneuf, R. A., Taylor, P. O. & Dunn, G. H. Absolute cross sections for electron-impact excitation of N_2^+. *Phys. Rev. A* **9,** 2545–2551 (1974).

27. Corkum, P. B. Plasma perspective on strong field multiphoton ionization. *Phys. Rev. Lett.* **71,** 1994–1997 (1993).

28. Goreslavsky, S. P. & Popruzhenko, S. V. Photoelectron velocity distribution at the time of ionization by elliptically polarized laser field. *Laser Phys.* **7,** 700–705 (1997).

29. Couairon, A. & Mysyrowicz, A. Femtosecond filamentation in transparent media. *Phys. Rep.* **441,** 47–189 (2007).

30. Ando, T. *et al.* Wave packet bifurcation in ultrafast hydrogen migration in CH_3OH^+ by pump-probe coincidence momentum imaging with few-cycle laser pulses. *Chem. Phys. Lett.* **624,** 78–82 (2015).

Acknowledgements

Author contributions

H.X. and K.Y. conceived the concept; E.L. performed the numerical calculations. H.X. and A.I. performed the experiments. H.X., E.L. and K.Y. analysed the data. The manuscript was prepared by H.X., E.L. and K.Y., and was discussed among all authors.

Additional information

Competing financial interests: The authors declare no competing financial interests.

Reprints and permission information is available online at http://npg.nature.com/reprintsandpermissions/

How to cite this article: Xu, H. *et al.* Sub-10-fs population inversion in N_2^+ in air lasing through multiple state coupling. *Nat. Commun.* 6:8347 doi: 10.1038/ncomms9347 (2015).